International Journal of Microwave and Wireless Technologies

cambridge.org/mrf

Accuracy study for over-the-air frequency synchronization of continuous wave signals

Thomas Dallmann[1] and Reiner Thomä[2]

[1]Radio Technologies for Automated and Connected Vehicles Research Group at Thüringer Innovationszentrum Mobilität, Technische Universität Ilmenau, Ilmenau, Germany and [2]Electronic Measurements and Signal Processing Group at Thüringer Innovationszentrum Mobilität, Technische Universität Ilmenau, Ilmenau, Germany

Research Paper

Cite this article: Dallmann T, Thomä R (2024) Accuracy study for over-the-air frequency synchronization of continuous wave signals. *International Journal of Microwave and Wireless Technologies*, 1–7. https://doi.org/10.1017/S1759078724001090

Received: 12 February 2024
Revised: 16 September 2024
Accepted: 5 October 2024

Keywords:
5G; 6G; Ad-Hoc; frequency offset; ICAS; Kuramoto; Over-the-air; radar; Synchronization

Corresponding author: Thomas Dallmann; Email: thomas.dallmann@tu-ilmenau.de

Abstract

Future communication and radar sensing systems will require synchronization methods which are more versatile in terms of the systems involved in the synchronization process. We present an over-the-air frequency synchronization algorithm based on the standard and the generalized Kuramoto model which uses continuous wave (CW) signals. In contrast to other approaches, all nodes of the network participate equally, and synchronization can even be achieved in presence of a non-cooperative node. By changing the parameters of the radar or by modifying the synchronization algorithm, synchronization accuracy can be adjusted as well. All claims are supported by measurements conducted with CW radars. It will be demonstrated that our algorithm enables synchronization accuracies down to 1.92 ppb and thus could provide sufficient accuracy for velocity measurements on pedestrians.

Introduction

With the advent of integrated communication and sensing (ICAS) and its potential integration into 6G, new possibilities emerge for expanding this technology: Systems that are designed for both communication and radar sensing tasks can be used to realize cooperative sensor networks, which not only share environmental information between each other, but also work together by realizing multistatic radar networks. This allows to increase diversity gain and thus the probability of detection of radar targets, to cover blind spots and to improve target classification capabilities. Applications like automated driving and lower airspace surveillance would highly benefit from these improvements: To increase road traffic safety and to enable a smoother and thus more environmentally friendly traffic flow, comprehensive perception of even complex environments like urban road intersections is required. Similarly, imminent heavy use of airspace by drones requires surveillance systems which are able to cover widespread areas populated along all three spatial directions [1].

The realization of ICAS networks requires synchronization methods which in perspective not only enable control of wireless access to avoid interference, but realize coherent operation of all network nodes. This would permit the simultaneous operation of several transmitters and thus a targeted illumination of the environment as well as multistatic operation of distributed transceivers [2]. Second, to enable also the integration of mobile nodes, the use of over-the-air synchronization is necessary. Finally, synchronization should be possible independent from the nodes involved so that a cooperative operation can be realized in as many scenarios as possible. Although synchronization methods were investigated both for communications and radar in the past, they mostly rely on hierarchical master-slave configurations, thus requiring either the presence of a master node or clock [3–6], or demand cooperative behavior from all nodes for successful synchronization [7–9].

If the measurement of target velocities shall be enabled between distributed nodes, special requirements are placed on the synchronization accuracy of frequency synchronization algorithms: A pedestrian radially moving toward a monostatic radar at a walking speed of $v = 1$ m/s causes a Doppler shift of approx. $f_D = 2f_c v/c_0 = 527.03$ Hz at $f_c = 79$ GHz. To resolve such targets, synchronization accuracies below $f_D/f_c = 6.67$ ppb are required, possibly even less if the target is not moving radially toward the radar or if a bistatic configuration is used. Here, the unit ppb refers to "parts per billion" and agrees with the factor 10^{-9}. The mentioned accuracy is well below the requirements of modern communication standards like 5G new radio (NR), where frequency synchronization accuracies of 50 ppb are necessary [10]. However, if ICAS functionalities are to become part of future 6G technology, the aforementioned much stricter requirements for synchronization will have to be met.

In this publication, we will focus on an over-the-air frequency synchronization method based on the standard and generalized Kuramoto self-synchronization model [11, 12]. An earlier version of this paper was presented at the 20th European Radar Conference (EuRAD)

2023 and was published in its proceedings [13]. Our method has the advantage that it does not need a master-slave structure between the nodes, since all contribute in the same way to the synchronization process. Moreover, it can even work if one of the nodes does not participate in the synchronization process and therefore is non-cooperative. This behavior was already investigated in theory and by simulation in prior publications, which focused on the synchronization of pulse repetition frequencies of pulse radars [14, 15]. Here, we will apply this approach to correct the carrier frequency offset (CFO) of continuous wave (CW) signals by proposing adapted and generalized versions of the Kuramoto model and verify it by means of measurements. Such CW signals are widespread both in communications and radar: They are part of 5G NR, where they are used for channel estimation and denoted as pilot symbols or reference signals [16]. In radar technology, they can also be found in CW radars for measuring Doppler frequencies, as well as in frequency modulated CW (FMCW) radars, which often transmit CW signals between chirps. For this reason, the waveform is a good choice for applying self-synchronization to it. In comparison to [13], we added the discussion of the generalized Kuramoto model and compare its performance to the standard model.

In the following section, we introduce the Kuramoto model and discuss why it must be adapted for the use of CW signals. Afterward, we propose our self-synchronization algorithm. Additionally, we introduce different synchronization functions that generalize the standard Kuramoto model. In "Measurements and results" section, we present the measurement setup we use to test the algorithm and discuss the measurement results. Finally, we conclude by naming future challenges.

Theoretical background

In [11], Kuramoto described the coupling between a set of harmonic oscillators with

$$\varphi'_m = \omega_{m,0} + \varepsilon_m \sum_{n=1}^{M} g(\psi_{nm}), \tag{1}$$

where

$$\psi_{nm} = \varphi_n - \varphi_m. \tag{2}$$

φ_m is the phase of harmonic oscillator m and φ'_m is its instantaneous frequency. Moreover, ε_m describes the coupling strength between oscillators, $\omega_{m,0}$ is the initial angular frequency of oscillator m, and ψ_{nm} agrees with the phase difference between oscillators n and m. Equation (1) describes the generalized version of the Kuramoto model, where $g(x)$ is an arbitrary 2π-periodic function. The standard model as proposed by Kuramoto approximates $g(x)$ with

$$g_S(x) = \sin x. \tag{3}$$

For two oscillators, it simplifies to

$$\varphi'_1 = \omega_{1,0} + \varepsilon_1\, g(\psi_{21}), \tag{4}$$

$$\varphi'_2 = \omega_{2,0} + \varepsilon_2\, g(\psi_{12}). \tag{5}$$

For $g(x) = g_S(x)$ and by setting $\psi'_{nm} = 0$, it follows:

$$\psi'_{nm} = \arcsin\left(\frac{\omega_{n,0} - \omega_{m,0}}{\varepsilon_1 + \varepsilon_2}\right). \tag{6}$$

Since the argument of the arcsine must be $\in [-1, 1]$, the following synchronization criteria can be derived [14]:

$$\varepsilon_1 = \gamma_1 \left|\omega_{2,0} - \omega_{1,0}\right| = 2\pi\gamma_1 \left|f_{2,0} - f_{1,0}\right|,\ \gamma_1 \geq 1, \tag{7}$$

$$\varepsilon_2 = \gamma_2 \left|\omega_{1,0} - \omega_{2,0}\right| = 2\pi\gamma_2 \left|f_{1,0} - f_{2,0}\right|,\ \gamma_2 \geq 1. \tag{8}$$

This means that synchronization can be successful if the coupling factor ε_l is $\gamma_l \geq 1$ times larger than the initial angular frequency difference between the oscillators (for $l \in \{1, 2\}$). In principle, these equations could be directly used for frequency alignment of CW signals, since they are meant for synchronization of harmonic oscillator frequencies. However, in practice it is unlikely that this approach can be used: The Kuramoto model describes a continuous process, which means that the oscillator frequencies must be adjusted within a fraction of the signal period $T_m = 2\pi/\varphi'_m$ to come close to continuous behavior. For a CW signal of several GHz, this update rate is much too high to be realized with a digital circuit. In addition, continuous adjustment of the oscillator frequency is inconsistent with the way radar and communication systems are operated: A CW radar must take multiple samples while transmitting a CW signal of constant frequency to be able to determine the velocity of targets. Similarly, pilot symbols in communication protocol packets remain at a constant frequency and vary from packet to packet only. For this reason, continuous adjustment of the CW signal frequency is neither desirable nor technically feasible.

Synchronization of pilot tones

Instead, we propose a self-synchronization method based on CW signals whose frequency is kept constant during time duration T. In the following, a CW signal of constant frequency and duration T will be denominated as a pilot tone. If pilot tones of different frequencies follow one after another, the phase of the signal generated by system m can be described after a pilot tones by

$$\varphi_{m,a} = \int_0^{aT} \omega_m(t)\,\mathrm{d}t = T\sum_{p=0}^{a} \omega_{m,p} = 2\pi T \sum_{p=0}^{a} f_{m,p}, \tag{9}$$

where $f_{m,p}$ is the frequency of the pth pilot tone of system m. Rewritten as an update equation, it becomes

$$\varphi_{m,a} = \varphi_{m,a-1} + 2\pi T f_{m,a}, \quad \varphi_{m,0} = 0. \tag{10}$$

In the following, it will be assumed without loss of generality that system 1 is the system under control and system 2 is the interferer. If applying the Kuramoto model described by (4), the frequency of the oscillator of system 1 is adjusted according to

$$f_{1,a+1} = f_{1,0} + \epsilon_1\, g(\psi_{21,a}), \tag{11}$$

where $\varepsilon_1 = 2\pi\epsilon_1$. By substitution of (10), $\psi_{21,a}$ can be determined to

$$\psi_{21,a} = \varphi_{2,a} - \varphi_{1,a} \tag{12}$$

$$= \varphi_{2,a-1} - \varphi_{1,a-1} + 2\pi T f_{2,a} - 2\pi T f_{1,a} \tag{13}$$

$$= \psi_{21,a-1} + 2\pi T f_{\Delta,a}. \tag{14}$$

Here, $f_{\Delta,a}$ is the CFO between the pilot tones of system 2 and system 1. The calculation of $\psi_{21,a}$ corresponds to the sampling of the phase of a time-varying signal. To fulfill the Nyquist sampling criterion in this case, $Tf_{\Delta,a} \leq 0.5$ is required. This is achieved for (14) with an arbitrary scaling factor κ:

https://doi.org/10.1017/S1759078724001090 Published online by Cambridge University Press

$$\psi_{21,a} = \psi_{21,a-1} + 2\pi \frac{T}{\kappa} f_{\Delta,a}. \tag{15}$$

Now, the Nyquist criterion $Tf_{\Delta,a}/\kappa \leq 0.5$ holds. Since $f_{\Delta,a} \leq 0.5 f_{\mathrm{ADC}}$ must be equally satisfied, where f_{ADC} is the sampling rate of the radars analog-to-digital converter (ADC), it can be derived:

$$\kappa \geq Tf_{\mathrm{ADC}} \quad \Rightarrow \quad \kappa = N_{\mathrm{s}} Tf_{\mathrm{ADC}},\ N_{\mathrm{s}} \geq 1. \tag{16}$$

By substitution into (15), it follows

$$\psi_{21,a} = \psi_{21,a-1} + 2\pi \frac{f_{\Delta,a}}{N_{\mathrm{s}} f_{\mathrm{ADC}}}. \tag{17}$$

N_{s} will be denoted as sampling factor in the following.

The synchronization procedure therefore works out as follows: During time duration T, system 1 records a pilot tone of the interferer and estimates the CFO $\hat{f}_{\Delta,1} = \hat{f}_2 - f_1$, e.g. by Fourier transformation of the recorded signal. For CW radars, this Fourier transformation is already part of the signal processing chain, since Doppler frequencies are determined in the same way. Afterward, the frequency $f_{1,a+1}$ of the next pilot tone is calculated using (11) after determining the phase difference $\psi_{21,a}$ with (17). After setting the new pilot tone frequency, the process starts again from the beginning.

It shall be noted that (11) and (14) are comparable to the equations for PRF synchronization in [14], with the biggest difference being the quantities used to determine $\psi_{21,a}$. However, if compared to [15], it becomes apparent that one term of $\psi_{21,a}$ is missing, which is required to compensate the occurrence of more than one or less than one pulse of the interfering radar during one pulse repetition period. Since it is assumed that the signal duration T is the same for both systems, the acquisition of the pilot tone takes the same amount of time, rendering the additional term unnecessary here. However, slightly different pilot tone durations are acceptable as long as two different pilot tones transmitted by the interfering radar do not mix up at the system under control, e.g. due to Fourier transform. This can be prevented with various strategies like synchronizing pilot tone durations, adding pauses in between the tones or advanced processing techniques to separate two subsequent tones received by the radar.

Standard vs. generalized Kuramoto model

$g(x)$ in (1) directly affects the synchronization process, since it determines how much the frequency of a pilot tone has to change depending on the phase difference between the tones. It therefore makes sense to identify other functions in addition to $g_{\mathrm{S}}(x)$ that could positively influence the synchronization process. Therefore, we investigate how synchronization can be accelerated.

Let $\psi_{21,\mathrm{sync}} = -\psi_{12,\mathrm{sync}}$ be the phase difference at which two pilot tone frequencies become synchronized, meaning that $\psi'_{21,\mathrm{sync}} = \psi'_{12,\mathrm{sync}} = 0$. If synchronization shall be achieved fast, two requirements must be fulfilled:

First, to quickly reach $\psi_{21,\mathrm{sync}}$, the phase difference ψ_{21} needs to change fast over time, meaning that ψ'_{21} must be maximized. From (4) and (5) follows:

$$\psi'_{21} = \varphi'_2 - \varphi'_1 = \omega_{2,0} - \omega_{1,0} - (\varepsilon_1 + \varepsilon_2)\, g(\psi_{21}). \tag{18}$$

Here, a strong phase change ψ'_{21} is only achieved if $|g(\psi_{21})|$ is close to its maximum value for most values of ψ_{21}.

Second, for values close to $\psi_{21,\mathrm{sync}}$, the frequency difference ψ'_{21} needs to change fast to quickly reach $\psi'_{21,\mathrm{sync}}$. From (18) can be derived that

$$\psi''_{21,\mathrm{sync}} = -(\varepsilon_1 + \varepsilon_2)\, g'(\psi_{21,\mathrm{sync}}). \tag{19}$$

Here, a strong frequency change $\psi''_{21,\mathrm{sync}}$ is only achieved if $|g'(\psi_{21,\mathrm{sync}})|$ is maximized. Since this requirement is independent from where $\psi_{21,\mathrm{sync}}$ is located, the strongest increase in the function even does not have to be at $x = 0$, as long as the function is still odd as required in "Theoretical background" section.

According to the last two requirements, $|g(\psi_{21})|$ should take the maximum value for all values of ψ_{21} except for $\psi_{21,\mathrm{sync}}$, where $|g'(\psi_{21,\mathrm{sync}})|$ must be maximum. Therefore, all requirements can be ideally achieved with the sign function

$$g_{\mathrm{sgn}}(x) = \begin{cases} +1 & x \geq 0 \\ -1 & x < 0 \end{cases},\ x \in [-\pi, \pi). \tag{20}$$

However, substitution of (20) into (18) shows that this function leads to an oscillation between $\omega_{2,0} - \omega_{1,0} \pm (\varepsilon_1 + \varepsilon_2)$, causing a degradation in synchronization accuracy. Therefore, the choice of a suitable $g(\psi_{nm})$ points to a compromise between fast and accurate synchronization.

To investigate this, two different functions for the generalized Kuramoto model will be used, which are

$$g_P(x) = \sin(x)^P \tag{21}$$

and

$$g_{\Sigma,P}(x) = \sum_{q=-Q}^{Q} \sin(x - mw)^P, \tag{22}$$

where P is odd and w, Q are given in the Appendix. Examples for both functions are shown in Fig. 1 and Fig. 2, where the function amplitude is given as dimensionless quantity. It becomes apparent that for $g_P(x)$, the peak around $\pm\pi/2$ gets narrower and steeper with increasing P, thus fulfilling the second requirement. For $g_{\Sigma,P}(x)$, a plateau is formed with steep slopes with increasing P, thus fulfilling both requirements. Moreover, the similarity to g_{sgn} increases with higher values of P. It should be noted that also other functions that fulfill one or both requirements could have been selected, such as the Fourier series of a square wave function. The two functions in this paper were chosen mainly for convenience, as they can be set with a single parameter and allow a better comparison with each other due to their similarity.

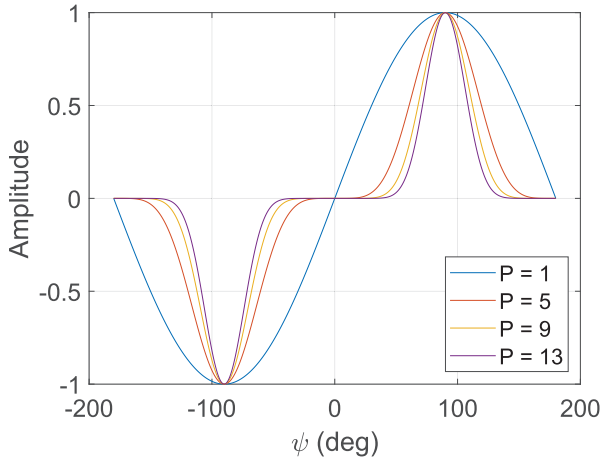

Figure 1. $g_P(x)$ for $x \in [-180°, 180°]$ and different values of P.

https://doi.org/10.1017/S1759078724001090 Published online by Cambridge University Press

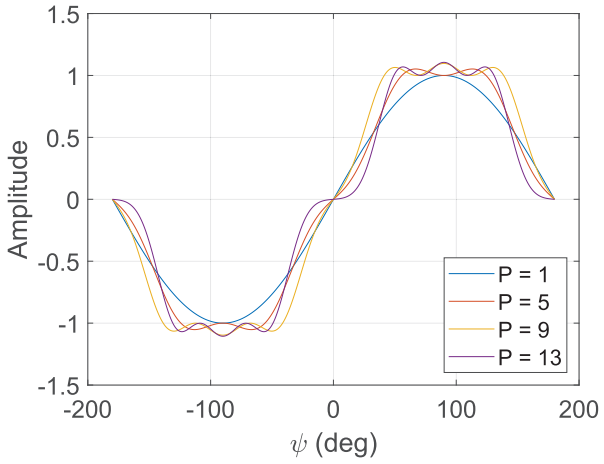

Figure 2. $g_{\Sigma,p}(x)$ for $x \in [-180°, 180°]$ and different values of P.

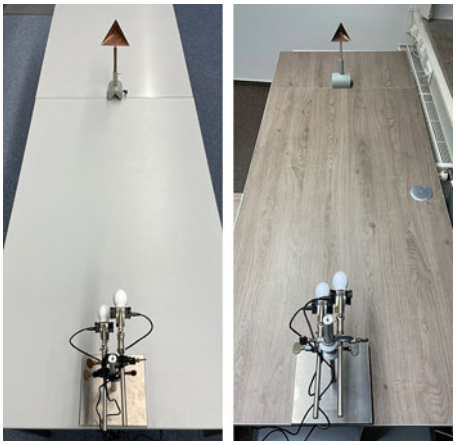

Figure 3. Measurement setups. Left: Setup realized for the standard Kuramoto model. Right: Setup realized for the generalized Kuramoto model.

In the following, both functions will be used for synchronization processes between two CW radars.

Measurements and results

To test the proposed synchronization method, two monostatic FMCW radars manufactured by Fraunhofer Institute for High Frequency Physics and Radar Techniques FHR covering a chirp bandwidth from 68 GHz to 93.5 GHz and featuring an ADC sampling rate of $f_{\mathrm{ADC}} = 1$ MHz were used. For this experiment, they were operated as CW radars around 79 GHz. As shown on both images in Fig. 3, the radars, recognizable by their white lens antennas, were mounted to supports and pointed in the same direction toward a trihedral located at a distance of approx. 1.5 m. Radar 1 operates by recording measurement data during time T, applying a Hamming window onto the recorded data set, performing a Fourier transform and using thresholding for target detection. Moreover, static targets were filtered out by subtracting the mean from the time domain signal before Fourier transformation to suppress reflections caused by antenna mismatch and static surrounding. The frequency of the highest peak found by a maximum search is used as an estimate for the CFO $\hat{f}_{\Delta,a}$. This value is subsequently used to calculate $f_{1,a+1}$ and to adjust the CW frequency of radar 1. Radar 2 operates the same way, meaning that both radars transmit simultaneously during measurements. After updating their CW frequencies, both radars repeat the process from the beginning. Due to hardware limitations, only the absolute frequency value $|f_{\Delta,a}|$ can be measured, making it necessary to hand over the sign to the signal processing methods of both radars as a-priori information after each measurement. This sign is directly calculated from the values $f_{1,a+1}$ used to set the CW frequencies of both radars.

In the following, three different quantities will be discussed, the definition of which we give here. The CFO between both radars after synchronization $f_{\Delta,\mathrm{sync}}$ is defined to the largest difference between frequencies observed after synchronization took place. The synchronization accuracy given in ppb is the aforementioned CFO in relation to the carrier frequency at 79 GHz. The number of pilot tones or iterations until synchronization is achieved I_{sync} is measured to be the number of tones until the CFO falls below $f_{\Delta,sync}$ for the first time.

Standard Kuramoto model

Initially, the standard model with $g(x) = g_{\mathrm{S}}(x)$ will be used. Measurements were carried out using the setup shown on the left side of Fig. 3. $f_{1,0}$ of radar 1 was set to 79 GHz and $f_{2,0}$ of radar 2 was set 0.4 MHz above $f_{1,0}$. The sampling factor was chosen to $N_{\mathrm{s}} = 64$. The pilot tone duration was set to $T = 4$ ms, resulting in $Tf_{\mathrm{ADC}} = 4000$ samples per pilot tone. While keeping $\gamma_1 = 1.2$, the value of γ_2 was varied between 0 and 9.6. In Fig. 4, the variation of $f_{1,a}$ (dashed lines) and $f_{2,a}$ (solid lines) is shown for 64 pilot tones. For $\gamma_2 = 1.2$, both radars adjust their CW frequencies using the same gamma factor. Due to this, they synchronize to a frequency lying approximately in the middle of $f_{1,0}$ and $f_{2,0}$. For $\gamma_2 = 2.4$ to $\gamma_2 = 9.6$, radar 2 forces the synchronization process to frequencies which are closer to $f_{1,0}$. The downside of choosing high values for γ_2 is a high frequency fluctuation, resulting in low synchronization accuracy. However, it comes with the advantage that synchronization is achieved after a lower number of pilot tones. For $\gamma_2 = 0$, radar 2 does not adjust its CW frequency. Nevertheless, synchronization still takes place, since radar 1 adjusts its frequency to $f_{2,0}$. This demonstrates that self-synchronization can still be successful if one system is non-cooperative.

Next, $f_{1,0}$, $f_{2,0}$, and T were kept the same and $\gamma_1 = \gamma_2 = 1.2$ was chosen. N_{s} was varied between the values 16, 64, and 256.

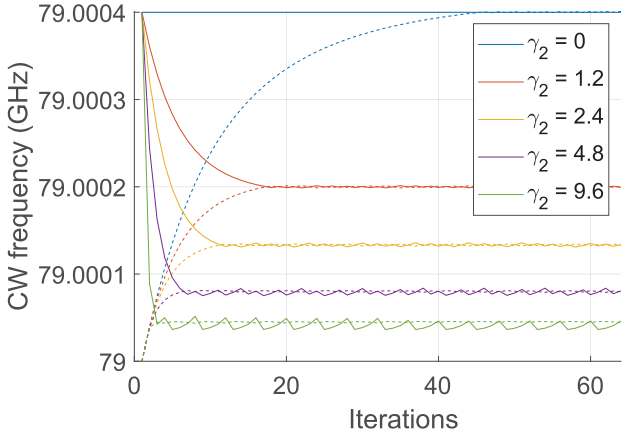

Figure 4. Synchronization process for different γ_2.

https://doi.org/10.1017/S1759078724001090 Published online by Cambridge University Press

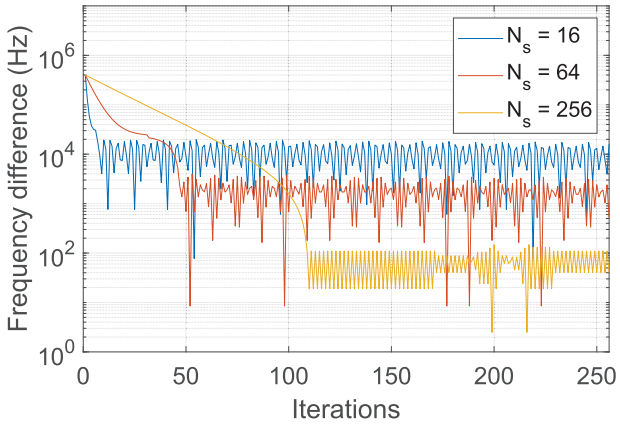

Figure 5. Synchronization process for different N_s.

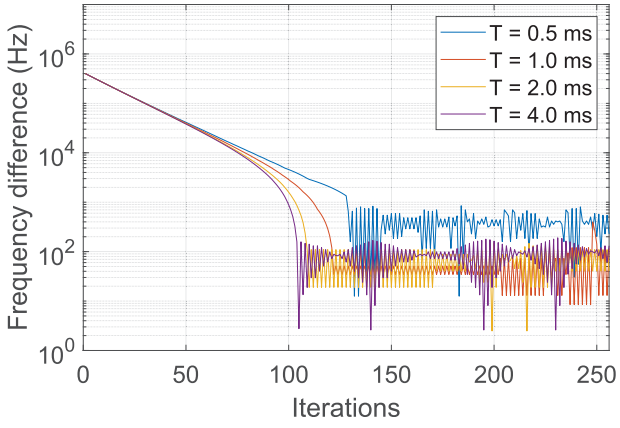

Figure 6. Synchronization process for different T.

In Fig. 5, the absolute frequency difference $|f_{\Delta,a}|$ is shown on logarithmic scale for 256 pilot tones on the y-axis, whereas the number of iterations is shown as dimensionless quantity on the x-axis. It can be seen that higher synchronization accuracies are achieved if a higher sampling factor is chosen: For $N_s = 16$ the CFO $f_{\Delta,sync}$ is below 19.73 kHz, agreeing with a synchronization accuracy of 256.23 ppb, for $N_s = 64$ it is below 3.77 kHz, agreeing with a synchronization accuracy of 48.96 ppb and for $N_s = 256$ it is below 147.6 Hz, agreeing with a synchronization accuracy of 1.92 ppb. However, better synchronization accuracies come at the price of a slower synchronization process: For $N_s = 16$, synchronization is achieved after $I_{sync} = 7$ pilot tones, for $N_s = 64$ after $I_{sync} = 47$ pilot tones and for $N_s = 256$ after $I_{sync} = 109$ pilot tones.

Afterward, $N_s = 256$ was chosen while keeping $f_{1,0}$, $f_{2,0}$, γ_1, and γ_2 the same as before. Time duration T was varied between 0.5 ms, 1.0 ms, 2.0 ms and 4.0 ms. The use of longer pilot tones affects the estimation of the CFO $|f_{\Delta,a}|$ because it reduces the frequency point spacing in the frequency domain. Longer pilot tones therefore allow $|f_{\Delta,a}|$ to be estimated more accurately. This can be seen in Fig. 6, where using $T = 0.5$ ms resulted in a lower synchronization accuracy compared to $T \geq 1.0$ ms. Nevertheless, the synchronization accuracy could not be improved for values above $T = 1.0$ ms, possibly because the chosen sampling factor $N_s = 256$ is the dominant influence on synchronization accuracy from there on. Thus, sampling factors smaller than $N_s = 256$ would possibly allow for time durations of $T = 0.5$ ms and smaller. Since the radars are limited to a minimum time duration of $T = 0.4$ ms, this could not be investigated.

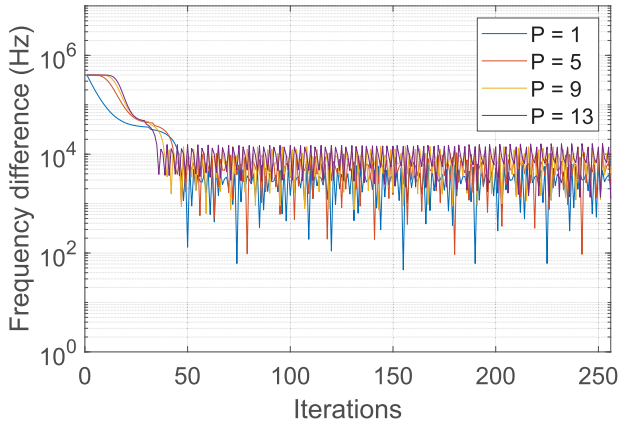

Figure 7. Synchronization process for $g_P(x)$.

Generalized Kuramoto model

After studying the standard model, its generalized version was investigated by application of $g_P(x)$ and $g_{\Sigma,P}(x)$. As parameters, $f_{1,0} = 79$ GHz, $f_{2,0} = f_{1,0} + 0.4$ MHz, $N_s = 64$, $\gamma_1 = \gamma_2 = 1.2$, and $T = 4$ ms were chosen. Since the experiments were conducted at a later date, the last setup was reproduced as shown of the right side of Fig. 3. First, $g_P(x)$ was tested for different values of P, resulting in the curves shown in Fig. 7, showing the absolute frequency difference $|f_{\Delta,a}|$ on logarithmic scale for 256 iterations on the y-axis and the number of iterations as dimensionless quantity on the x-axis again. In comparison to the standard model, the number of required pilot tones can be reduced by increasing P, achieving a reduction from $I_{sync} = 47$ to $I_{sync} = 35$ pilot tones from $P = 1$ to $P = 13$. In contrast, $f_{\Delta,sync} = 6.49$ kHz increases to $f_{\Delta,sync} = 16.43$ kHz, agreeing with synchronization accuracies of 82.15 ppb and 207.97 ppb, respectively. The results show that although faster synchronization can be achieved, the added value of using $g_P(x)$ is limited. The reason can be seen from the progression of the curves: For higher values of P, the curves start the synchronization process later, but achieve synchronization faster afterward, leading to a small improvement in total. Since $g_P(x)$ only fulfills the second requirement described in "Standard vs. generalized Kuramoto model" section, a significant part of the signals shown in Fig. 1 is close to zero and therefore prevents a fast progression of ψ_{21}, delaying the synchronization process.

In comparison, $g_{\Sigma,P}(x)$ outperforms $g_P(x)$ as is shown in Fig. 8. Here, a reduction from $I_{sync} = 51$ to $I_{sync} = 27$ pilot tones from $P = 1$ to $P = 9$ is achieved. $f_{\Delta,sync} = 8.26$ kHz increases to $f_{\Delta,sync} = 16.49$ kHz with synchronization accuracies of 104.56 ppb and 208.73 ppb, respectively. This shows that a comparable accuracy could be reached with a lower number of pilot tones if compared with $g_P(x)$ for $P = 13$. Although the synchronization speed is similar for $P = 9$ and $P = 13$, this behavior seems to be an exception, as a further reduction in the number of required pilot tones can be seen for $P = 17$. Due to the better performance of $g_{\Sigma,P}(x)$ in comparison to $g_P(x)$ since the aforementioned first criterion is not fulfilled for $g_P(x)$, the focus is placed on $g_{\Sigma,P}(x)$ in the following.

https://doi.org/10.1017/S1759078724001090 Published online by Cambridge University Press

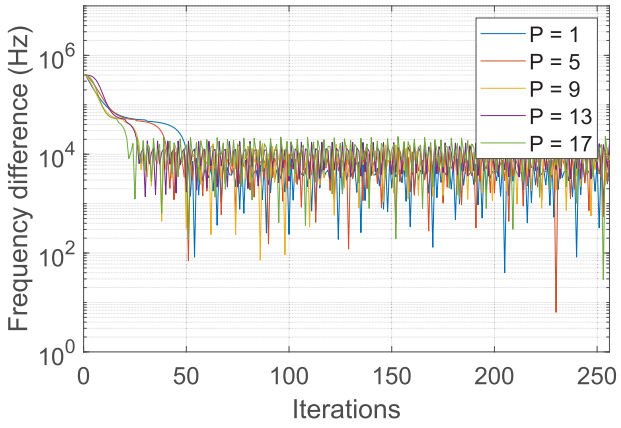

Figure 8. Synchronization process for $g_{\Sigma,P}(x)$.

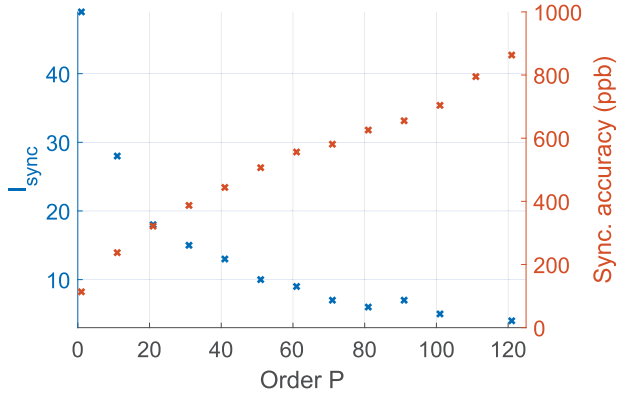

Figure 9. Change in synchronization speed and accuracy for $g_{\Sigma,P}(x)$.

Figure 9 allows to study the performance of $g_{\Sigma,P}(x)$. It shows both I_{sync} as well as the synchronization accuracy for different P values on the y-axes and the number of iterations as dimensionless quantity on the x-axis. The nonlinear dependency of the number or required pilot tones on P hints at the added value of using the generalized model: For low values of P, a considerable synchronization speed-up can be achieved without a significant deterioration in synchronization accuracy. For higher values of P, this advantage is lost: Comparing Fig. 5 with $N_S = 16$ from last section with the results shown for $P = 61$ in Fig. 9, it becomes apparent that in both cases synchronization is achieved after $I_{\text{sync}} = 9$ tones, but the change of the sampling factor from $N_S = 64$ to $N_S = 16$ affects synchronization accuracy significantly less. This also becomes apparent from evaluating the product of I_{sync} and synchronization accuracy, which is highest for $P = 11$. It is therefore recommended to apply to the generalized Kuramoto model only small P values around $P = 11$ to gain an advantage in terms of synchronization speed and accuracy.

A comparison of synchronization performance for $g_P(x)$ and $g_{\Sigma,P}(x)$ is shown in Table 1. The table also contains results from the last section for comparison. It should be noted that by comparing the three cases where $N_S = 64$ and $P = 1$, a significant variation in synchronization accuracy can be determined. This shows that the synchronization is sensitive to environmental influences, leading to performance fluctuations. However, during the experiments, consideration was given to changing N_S and P over a range of values that would result in significant changes in synchronization accuracy, which is why the discussed results retain their validity.

Table 1. Performance comparison of different synchronization parameters

Figure	N_S	P	I_{sync}	Sync. accuracy
5	16	1	7	256.23 ppb
	64		47	48.9 ppb
	256		109	1.92 ppb
7	64	1	47	82.15 ppb
		5	44	136.71 ppb
		9	39	181.14 ppb
		3	35	207.97 ppb
8	64	1	51	104.56 ppb
		5	44	136.71 ppb
		9	27	208.73 ppb
		13	27	234.81 ppb
		17	21	290.63 ppb

Conclusions

The results presented in the last section show that over-the-air self-synchronization of two CW radars can be carried out successfully, even if one radar is non-cooperative. In addition, frequency synchronization accuracies of 1.92ppb could be achieved which would enable the resolution of a pedestrian moving at 1 m/s. However, these accuracies come at the cost of a slower convergence of the pilot tone frequencies. A small number of pilot tones required to achieve synchronization is desirable because the time taken by these pilot tones is not available for coordinated use of both systems. It could be shown that sampling factor N_S, pilot tone duration T and synchronization function $g(x)$ affect both synchronization speed and duration. However, the results demonstrate that a balance must always be struck between the two criteria.

In highly dynamic scenarios, it is expected that changes in the environment will occur during the synchronization process that will require resynchronization. If the scenarios are additionally highly complex, such as in urban traffic situations or in maritime environments, the synchronization process can also be severely disturbed. For this reason, environments of higher complexity will be considered in the future to understand the influence of multipath and moving targets onto the synchronization process. As a very basic approach for frequency estimation based on thresholding and maximum search was used, it is likely that the synchronization accuracy can also be improved by applying curve fitting to the peak. Since two radars were used for the present study, the Kuramoto model was designed for the participation of two nodes. An extension to more nodes is conceivable and feasible and will also be addressed in the future. Nevertheless, the research in this publication paves the way for for these investigations by demonstrating that self-synchronization processes are suitable for the synchronization of communication and radar systems.

Acknowledgements. This work was supported by the German Research Foundation (Deutsche Forschungsgemeinschaft, DFG) through project

https://doi.org/10.1017/S1759078724001090 Published online by Cambridge University Press

"Coordinated multipoint operation for joint communication and radar sensing - JCRS CoMP" (project number 504990291).

Competing interests. The authors report no competing interests.

References

1. **Thomä R, Dallmann T, Jovanoska S, Knott P and Schmeink A** (2021) Joint communication and radar sensing: An overview. In *15th European Conference on Antennas and Propagation (EuCAP), Düsseldorf, Germany*.
2. **Thomä R and Dallmann T** (2023) Distributed ISAC systems – Multisensor radio access and coordination. In *2023 20th European Radar Conference (EuRAD), Berlin, Germany*.
3. **Chaloupka Z** (2017) Technology and standardization gaps for high accuracy positioning in 5G. *IEEE Communications Standards Magazine* **1**(1), 59–65.
4. **Omri A, Shaqfeh M, Ali A and Alnuweiri H** (2019) Synchronization procedure in 5G NR systems. *IEEE Access* **7**, 41286–41295.
5. **Dürr A, Böhm D, Schwarz D, Häfner S, Thomä R and Waldschmidt C** (2022) Coherent measurements of a multistatic MIMO radar network with phase noise optimized non-coherent signal synthesis. *IEEE Journal of Microwaves* **2**(2), 239–252.
6. **de Oliveira LG, Brunner D, Diewald A, Muth C, Schmalen L, Zwick T and Nuss B** (2023) Bistatic OFDM-based joint radar-communication: Synchronization, data communication and sensing. In *2023 20th European Radar Conference (EuRAD), Berlin, Germany*.
7. **Feger R, Pfeffer C, Scheiblhofer W, Schmid CM, Lang MJ and Stelzer A** (2013) A 77-GHz cooperative radar system based on multi-channel FMCW stations for local positioning applications. *IEEE Transactions on Microwave Theory and Techniques* **61**(1), 676–684.
8. **Kong S, Lee S, Kim C and Hong S** (2014) Wireless cooperative synchronization of coherent UWB MIMO radar. *IEEE Transactions on Microwave Theory and Techniques* **62**(1), 154–165.
9. **Dzvonkovskaya A, Helzel T, Petersen L and Gill E** (2015) Self-organized synchronization based on a chirp-sequence waveform for an HF ocean radar network. In *OCEANS 2015 - MTS/IEEE Washington, Washington, DC, USA*.
10. ETSI 3GPP (2021) 5G; NR; Base Station (BS) radio transmission and reception.
11. **Kuramoto Y** 1975 Self-entrainment of a population of coupled nonlinear oscillators. In *International Symposium on Mathematical Problems in Theoretical Physics*, H Araki (ed). Berlin, Heidelberg: Springer.
12. **Pikovsky A and Rosenblum M** (2015) Dynamics of globally coupled oscillators: Progress and perspectives. *Chaos: An Interdisciplinary Journal of Nonlinear Science* **25**(9), 9.
13. **Dallmann T and Thomä R** (2023) Mutual over-the-air frequency synchronization of continuous wave signals. In *2023 20th European Radar Conference (EuRAD), Berlin, Germany*.
14. **Dallmann T** (2020) Mutual over-the-air synchronization of radar sensors. In *14th European Conference on Antennas and Propagation (EuCAP), Copenhagen, Denmark*.
15. **Dallmann T** (2021) Sampling criteria for mutual over-the-air synchronisation of radar sensors. *Electronics Letters* **57**(18), 702–704.
16. **Carrera DF, Vargas-Rosales C, Azpilicueta L and Galaviz-Aguilar JA** (2020) Comparative study of channel estimators for massive MIMO 5G NR systems. *IET Communications* **14**(7), 1175–1184.

Appendix

$g_{\Sigma,P}(x)$ extends $g_P(x)$ by superimposing several of its peaks to realize plateaus. This is achieved by the summation in (22), where w describes the amount by which the peaks are to be shifted. $g_P(x)$ has half of its signal strength at

$$\sin(x)^P = \frac{1}{2} \;\Leftrightarrow\; x = \arcsin\left(\frac{1}{\sqrt[P]{2}}\right). \tag{A.1}$$

Since the peak is located at $\pi/2$, its beamwidth can be determined with

$$w = 2\left(\frac{\pi}{2} - x\right) = 2\left(\frac{\pi}{2} - \arcsin\left(\frac{1}{\sqrt[P]{2}}\right)\right). \tag{A.2}$$

Only a limited number of R peaks fits into the intervals $[-\pi, 0]$ and $[0, \pi]$. The highest integer number of peaks within these can be determined as follows:

$$R = \left\lfloor \frac{\pi}{w} - 1 \right\rfloor. \tag{A.3}$$

Based on this, the limits $\pm Q$ of the sum in (22) can be defined to $Q = (R-1)/2$.

Thomas Dallmann received the Dipl.-Ing. degree in electrical engineering from the RWTH Aachen University, Germany in 2010 and the Dr.-Ing. degree from RWTH Aachen University in 2017. From 2016 to 2022, he was with the Fraunhofer-Institute for High Frequency Physics and Radar Techniques FHR, Wachtberg, Germany and lead the Research Group Aachen in Aachen, Germany. There he was involved with the development of new sensor concepts and validation approaches for automotive radars. He is currently Junior Professor at Technische Universität Ilmenau, Ilmenau, Germany and responsible for the Radio Technologies for Automated and Connected Vehicles Research Group. His research is concerned with joint communication and radar sensing networks and virtual validation of automotive radars.

Reiner S. Thomä received the degrees in electrical engineering and information technology from TU Ilmenau, Germany. Since 1992, he has been a Professor at the same university. He has retired since 2018. In 2007, he received the Thuringian State Research Award for Applied Research and in 2014 the Vodafone Innovation Award, both for his contributions to high-resolution multidimensional channel sounding. In 2020, he received the European Association on Antennas and Propagation (EurAAP) Propagation Award "For pioneering the multi-dimensional description of the mobile radio channel by advanced signal-processing methods." He has contributed to several European and German research projects and clusters. His research interests include multidimensional channel sounding, propagation measurement and model based parameter estimation, MIMO system over-the-air testing in virtual electromagnetic environments, MIMO radar, passive coherent location, and integrated communication and sensing.

https://doi.org/10.1017/S1759078724001090 Published online by Cambridge University Press